Computers and Electronics in Agriculture 219 (2024) 108834

Contents lists available at ScienceDirect

Computers and Electronics in Agriculture

journal homepage: www.elsevier.com/locate/compag

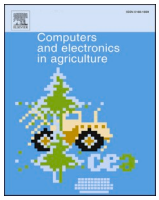

Original papers

Improved voxel-based volume estimation and pruning severity mapping of apple trees during the pruning period

Xuhua Dong [a], Woo-Young Kim [b], Zheng Yu [a], Ju-Youl Oh [e], Reza Ehsani [d], Kyeong-Hwan Lee [a,b,c,*]

[a] Department of Convergence Biosystems Engineering, Chonnam National University, Gwangju, Republic of Korea
[b] Agricultural Automation Research Center, Chonnam National University, Gwangju, Republic of Korea
[c] BK21 Interdisciplinary Program in IT-Bio Convergence System, Chonnam National University, Gwangju, Republic of Korea
[d] Department of Mechanical Engineering, University of California Merced, Merced, United States of America
[e] The Institute of Apple Utilization, Gyeongsangnam-do Agricultural Research and Extension Services, Geochang, Republic of Korea

ARTICLE INFO

Keywords:
Pruning severity
Tree volume
Multi-camera photogrammetry
3D reconstruction
Voxelization

ABSTRACT

Estimating tree volume is crucial for managing apple orchards, as it reflects the nutritional status and vigor of the trees. However, accurate assessment of tree volume in apple orchards is challenging due to their complex structure. This study introduces a novel method for three-dimensional volume calculation of individual apple trees. Our approach facilitates the determination of pruning severity by analyzing the limb-to-trunk volume ratio and enables the creation of detailed pre- and post-pruning maps. We utilized a lightweight multi-camera system to reconstruct 3D point clouds of the trees and developed a voxel-based algorithm for tree volume calculation. This algorithm includes steps for interior filling, edge voxel thinning, and interior refilling. We validated our algorithm on seven apple trees by comparing the calculated volumes with the ground truth, determined using the water displacement method. The results showed that our voxel-based algorithm was highly effective in accurately calculating individual tree volumes from 3D point clouds. The algorithm also demonstrated a high coefficient of determination (0.994) and a mean absolute percentage error of 2.919% in a linear regression analysis against the ground truth. Furthermore, we produced detailed tree volume and pruning severity maps for individual trees, both before and after pruning. In conclusion, this study offers an effective solution combining 3D imaging and volume calculation techniques to accurately estimate individual apple tree volumes, providing a quantitative assessment of pruning severity.

1. Introduction

Tree volume is particularly important for managing fruit trees in orchards, as it reflects the nutritional and vigor status of the trees and plays a role in decision making for dormant orchard management, such as pruning (Morgan et al., 2006; Lordan et al., 2015; Mahmud et al., 2021; Wang et al., 2021). However, measuring tree volume presents technical challenges, primarily due to irregular shapes and complex branching patterns of trees. Accurate quantification of tree volume involves time-consuming and labor-intensive methods, which are costly and impractical for large-scale application.

The volume of a fruit tree can be manually measured using xylometry methods, such as the water displacement method (Bienert et al., 2014). However, this method results in damage to the fruit tree and requires manual processing. Alternatively, model-based methods that utilize certain tree parameters can preserve the tree's integrity but are unable to determine its volume with high accuracy. For instance, a study used parameters such as tree height, stem diameter, and branching skewness in a prediction model to estimate the tree volume and obtained an accuracy of 25.58 % (Kankare et al., 2013).

Computer vision and three-dimensional (3D) remote sensing technologies can effectively overcome the limitations of existing manual and model-based methods. In addition to providing depth and structural information, a digital 3D model of complex branches can be reconstructed from the original physical world with identical characteristics. Compared with terrestrial laser scanning, multi-view imaging based on structure from motion (SFM) has the potential to reconstruct dense 3D point clouds of trees under field conditions using economically

* Corresponding author at: Department of Convergence Biosystems Engineering, Chonnam National University, Gwangju, Republic of Korea.
E-mail address: khlee@jnu.ac.kr (K.-H. Lee).

https://doi.org/10.1016/j.compag.2024.108834
Received 25 May 2023; Received in revised form 26 January 2024; Accepted 11 March 2024
Available online 16 March 2024

affordable and user-friendly RGBD cameras (Sun et al., 2020).

After trees are scanned by cameras, tree volume estimation can be efficiently and labor-sparingly performed using 3D point clouds. An increasing number of studies have confirmed the accuracy of tree above-ground biomass or tree volume measurements derived from 3D point clouds using Quantitative Structure Measurement (QSM) techniques. These measurements are validated by comparing them with values obtained through destructive methods (Burt et al., 2021; Demol et al., 2021a,b). The QSM is a geometric model that provides a hierarchical description of a tree's above-ground structure. For instance, TreeQSM, a tree model based on QSM, is capable of reconstructing a tree's structure using proximity relationships and geometric properties of the point set, which captures the topological branching structure of the tree. The topology of the entire tree is fitted to the point clouds of a single tree by fitting cylindrical surfaces to it, and the volume of each cylindrical section is calculated. This approach enables the calculation of the volume of the trunk and branches (Krishna Moorthy et al., 2020). Additionally, TreeQSM was further extended to the AdTree method, which has shown robustness across different types and sizes of trees (Fan et al., 2020a). However, QSM-type methods require a significant amount of computation and high-quality input data.

Tree skeleton extraction benefits from an understanding of the overall structure of trees (Bucksch et al., 2010; Yang et al., 2022; You et al., 2022). A single-tree-level volume estimation method was proposed, integrating skeleton extraction, topology optimization, and 3D reconstruction (Fan et al., 2023). This method addresses the problem of tree sagging branches, which can lead to misjudgments, by utilizing skeletonization processing to improve the accuracy of tree volume estimation. However, there may be discrepancies in the modeling results for trees with very complex branches, obscure branching, or branches with abnormal orientations. Additionally, the algorithm in their research requires extracting the skeleton points step by step in several iterations, which, although ensuring accuracy, consumes more memory and computation time. Similar to the QSM-based method, this algorithm demands high-quality input model data. The quality is particularly crucial for discontinuous fine branches in point clouds, as it can significantly impact the skeletonization process.

The point-cloud voxelization method is widely used for volume quantification of 3D point clouds (Xu et al., 2021). This method effectively simplifies the 3D point cloud of trees' complex branching structures into manageable volumetric units. A straightforward approach to calculate volume is to sum the volume of all filled voxels after mapping the 3D point cloud onto a voxel structure, which requires minimal computational resources. However, the volume estimation using this voxelization method still depends on a uniform voxel size. Consequently, a large voxel size often leads to significant overestimation of tree volume. Conversely, a small voxel size, smaller than the diameter of the stem or branch, may result in underestimation because it misses the voxels located inside large branches and stems, rendering them unusable for volume calculation (Qi et al., 2021). The conventional voxel method has not been able to determine a specific voxel size that would allow for accurate volume estimation. Moreover, the previous voxelization methods, which solely relied on adjusting voxel size, could not accurately assess both trunk and branch volumes of trees. Hosoi et al. (2013) improved the voxel-based method by filling the inner parts of the voxels. Although this approach reduced the error in volume estimation compared to the conventional method, the number and distribution of points in each voxel remained uncertain. Consequently, certain voxels were only partially filled with points, leading to volume overestimation, particularly in the small branches and the surface voxel of model.

Dual contouring (DC)-based technologies are popular for surface reconstruction and rendering in voxelization models (Hutchison et al., 2010). They generate smooth, high-accuracy surfaces from discrete inputs such as voxel grids. Unlike traditional DC methods, which compute vertex locations and edge crossings using hand-crafted functions reliant on hard-to-obtain surface gradients, neural dual contouring employs a neural network to predict these elements. This approach results in improved surface reconstruction accuracy and better feature preservation. However, the effectiveness of this technology is significantly influenced by the sparsity of the point cloud and the level of noise (Chen et al., 2022; Liu et al., 2023). For example, the fine and interlaced branches at the ends of apple trees often result in surface hollows or adhesion phenomena. Additionally, the voxel models created after surface reconstruction are not cube-shaped, necessitating additional steps for accurate volume estimation. Therefore, a key optimization for volume calculation algorithms is not just filling the internal empty spaces but also optimizing the side lengths of the voxels on the model's surface. This is crucial not only for accurate shape modeling but also for maintaining the original geometric characteristics of cubes to facilitate volume calculation.

Dormant pruning is necessary for orchard management to control tree vigor and achieve an appropriate balance between vegetative and reproductive growth to improve fruit yield and quality (Zai-long, 1983). Various pruning methods exist, including mechanical and manual pruning, based on different pruning strategies and rules (He and Schupp, 2018). However, the quantification of pruning severity is difficult owing to the complex branching structures of trees (Schupp et al., 2017). Previously, the limb-to-trunk ratio (LTR) was used to estimate pruning severity by dividing the sum of the cross-sectional area of all branches on a tree at 2.5 cm from their union to the central leader by the trunk cross-sectional area at 30 cm above the graft union (He and Schupp, 2018). However, manual measurement of the LTR index is generally time-consuming and laborious. Typically, volume changes in trees can directly reflect changes in biomass and vigor to a certain extent. If the LTR pruning severity index calculation is converted from an area to volume basis, the pruning magnitude can be conveniently calculated by comparing the limb-to-trunk volume ratio (LTVR) before and after pruning. The pruning operation mainly focuses on the rational removal of branches from fruit trees. However, to calculate the LTVR index, an accurate assessment of the volume of the fine branches is essential.

Therefore, in this study, a novel voxel-based algorithm is developed to accurately estimate the trunk and branch volume of fruit trees by filling inner voxels and compressing the voxels to adapt the point cloud shape and calculate LTVR to analyze the severity of different pruning methods. The specific objectives include (1) collecting images by designing a lightweight multi-camera system in the orchard and performing 3D reconstruction of all the trees therein; (2) developing a voxel-based volume calculation algorithm that includes interior filling, edge voxel thinning, and interior refilling; (3) comparing the proposed method with established methods; and (4) executing the proposed algorithm to estimate the entire volume and LTVR of all apple trees and perform pruning severity mapping.

2. Materials and methods

2.1. Experimental field and pruning methods

The study was conducted in a multi-variety apple orchard at the Apple Use Research Institute in Geochang city, Gyeongsangnam-do, South Korea (latitude: 35°43′9.07″N; longitude: 127°54′6.72″E). The selected experimental plot consisted of slender spindle type eight-year-old Honglo/M9 apple trees, which are commonly planted in orchards to achieve high tree densities and early production (Robinson et al., 1991). The slender spindle system allows for partial pruning mechanization, which can reduce the costs of pruning, hand thinning, and harvesting. The experimental plots comprised nine rows with varying tree intervals: 1 m intervals in rows 1–3, 1.5 m intervals in rows 4–6, and 2 m intervals in rows 7–9 (Fig. 1a). Each row was approximately 70 m in length, and the interval between neighboring rows was 4 m. Two pruning methods were employed: mechanical pruning and manual pruning. Rows 1, 4, and 7 were pruned mechanically using a non-selective pruning system, which involves a cutting machine being run

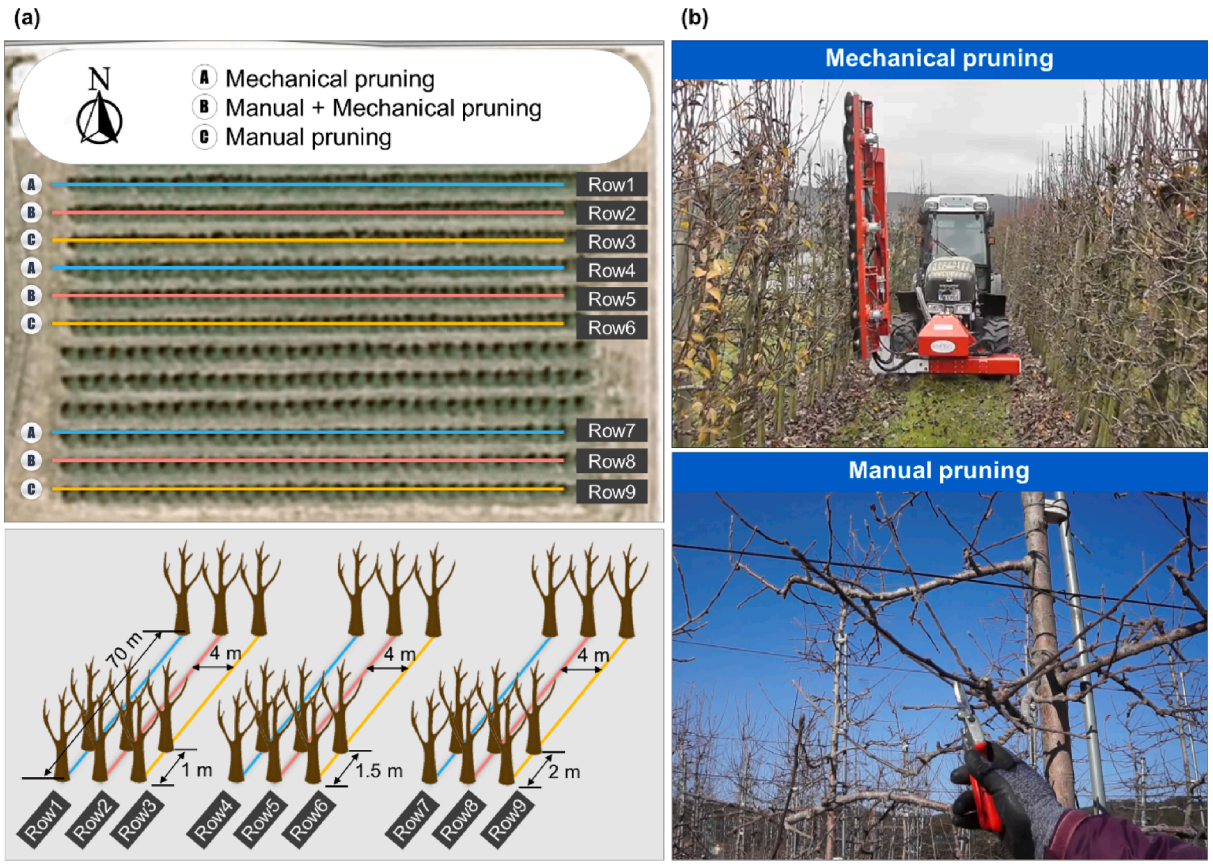

Fig. 1. Experiment field and pruning methods: (a) dimensions of the experimental test site, and (b) mechanical and manual pruning methods.

over the rows while maintaining a predetermined distance from the trees (He and Schupp, 2018). The pruning machine kept at a distance of 0.5 m from the tree trunk and at an angle of 10 degrees from the tree trunk. Rows 3, 6, and 9 were pruned manually by experienced growers, taking into consideration illumination and tree-vigor balance based on the fruit tree pruning strategy. Rows 2, 5, and 8 underwent a combination of mechanical and manual pruning. Initially, the trees were pruned by the machine, and then the insides of the trees were manually repruned by the growers (Fig. 1b).

2.2. Reconstruction of 3D point cloud images

A multi-camera system consisting of five GoPro 7 cameras (GoPro Inc., San Mateo, CA) was mounted on a single aluminum profile with a vertical spacing of 0.8 m between cameras, as shown in Fig. 2(a). The system was mounted on a vehicle and moved at a speed of 0.5 ms^{-1} between rows, scanning both sides of apple trees in the orchard. The cameras were set to record 4 k (4, 000 × 3, 000 pixel) resolution video at 30 frames per second (FPS) with a wide field of view (122.6° × 94.4°). Therefore, each camera captured a view of a 3.65m × 2.16m tree plane

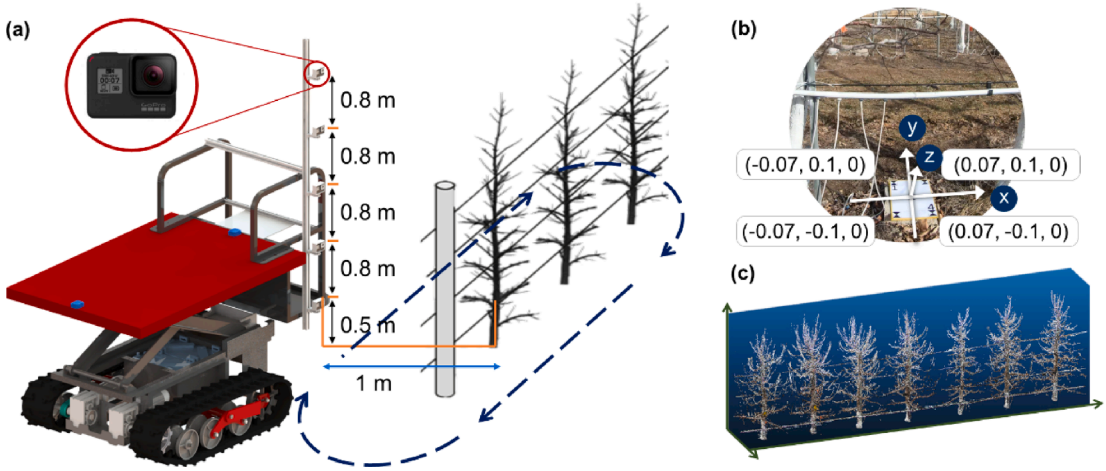

Fig. 2. Configuration of 3D point cloud image acquisition in the apple orchard: (a) image acquisition system consisting of five GoPro cameras scanning both sides of the trees, (b) a scale bar used to establish a local 3D Cartesian coordinate system and calibrate the size of the reconstructed 3D point cloud, and (c) a reconstructed point cloud image containing approximately 15 million points.

at a distance of 1 m. The camera configuration and layout ensured that the views of every two adjacent images overlapped by more than 60% in the vertical direction, which was optimal for 3D reconstruction. A total of 365 trees were scanned. The pre-pruning images were acquired on February 03, 2021, and the post-pruning images were collected on February 23, 2021, both being sunny days.

To reconstruct the 3D point cloud image, a hand-made scale cardboard was positioned at each tree row and captured by the cameras during image acquisition (Fig. 2b). The rectangular scale cardboard comprised four markers, allowing the establishment of a local 3D Cartesian coordinate system with coordinates assigned to each marker, such as (−0.07, 0.1, 0), (0.07, 0.1, 0), (0.07, −0.1, 0), and (−0.07, −0.1, 0). The rectangle measured 0.14 m in length and 0.2 m in width, therefore corresponding to an actual physical scale and serving to calibrate the size of the 3D point cloud. As shown in Fig. 2(b), the x-axis was aligned with the tree row direction. The y-axis formed a 90° angle with the x-axis on the ground, and the z-axis pointed upward, aligning with the direction of the tree trunk.

The 3D model of apple trees was generated with the traditional multi-view SFM algorithm based on bundle adjustment using Agisoft Metashape Professional software (v1.8.4, Agisoft LLC, St. Petersburg, Russia). This involved three primary steps: feature point matching, camera pose estimation, and 3D reconstruction. The images were obtained from the recorded video with a sampling of every 5 frames. For the image alignment operation, the upper limits were set to 40,000 key points and 4,000 matching points for each image. Owing to the presence of identical feature points on the cardboard, which were captured by the bottom cameras on both sides of the trees, the images from both sides of the trees could be matched effectively. The SFM algorithm processing based on bundle adjustment was executed to calculate the camera pose, and the four markers on the rectangular scale cardboard were manually masked in images to transform the original coordinates to the target coordinates. A mild depth filter was applied to eliminate outlier points resulting from poor input imagery due to alignment and focus issues (Tinkham and Swayze, 2021). Finally, a dense 3D point cloud was reconstructed using the ultra-quality mode (Fig. 2c).

2.3. Tree volume calculation

The methodology for calculating tree volume, as illustrated in Fig. 3, comprises the following steps: (1) extraction of individual trees, which includes preprocessing of the 3D point cloud, denoising, and voxelization; (2) calculation of trunk, branch, and overall tree volume using the proposed voxel-based algorithm; and (3) mapping of the tree volume and pruning severity onto an actual orchard image.

2.3.1. Preprocessing and voxelization of 3D point cloud

In this study, we focused on developing a novel method for tree volume calculation. Therefore, the extraction of individual trees was manually executed using CloudCompare V2.12, which is an open-source software for 3D point cloud processing with several advanced algorithms, such as resampling, registration, statistical computation, and interactive segmentation (Girardeau-Montaut, 2016). After removing the ground and tree supporting devices in the 3D point cloud and extracting the individual trees, the space sampling tool in CloudCompare was used to downsample the 3D point cloud of every tree and maintain the minimum distance between points from 0.37 mm to 1 mm. Additionally, a statistical-based filter was used to eliminate noise and outliers from the 3D point cloud (Han et al., 2017). The number of points used for mean distance estimation and the standard deviation multiplier threshold in the statistical-based filter were set to 50 and 0.5, respectively. The size of the tree's point could be significantly reduced from its original size (62 ~ 107 MB) to the filtered size (8 ~ 22 Mb), which greatly saved computing resources and improved processing speed. After calculating the volume of the entire apple tree, the 3D point cloud of each tree was manually segmented into trunk and branch parts. The proposed algorithm is based on the voxelization method depicted in Fig. 3.

2.3.2. Interior filling of the 3D voxel model

The voxel-based method employs 3D grids with a specific voxel size to organize the discrete 3D point cloud of individual trees and adds the volume of all filled voxels to estimate the tree volume. Each filled voxel contains at least one point, named as an edge voxel, and the 3D voxel model is divided into different layers in the Z-direction (Fig. 4). However, setting a small voxel size to obtain a high-quality 3D voxel model can cause the inner voxels, named as occluded voxels, in the stem and large branches that do not contain any points in the tree to be missed in the volume calculation, resulting in an underestimated volume. Therefore, to improve the accuracy of the volume calculation, the identification of occluded voxels and the interior filling of the 3D voxel model are necessary. The following steps were taken to detect the occluded voxels:

Step 1: The voxels in each column of the k-th layer are scanned from X_{min} to X_{max} in the Y-direction (Fig. 4a). The voxels $c_{ijk}(x_i, y_j, z_k)$ in this column of x_i are marked if the edge voxels of the tree existed in this Y-direction.
Step 2: Furthermore, the voxels in each row of the k-th layer are scanned from Y_{min} to Y_{max} in the X-direction (Fig. 4b). The voxels $c_{ijk}(x_i, y_j, z_k)$ in this row of y_j are marked if the edge voxels of the tree existed in this X-direction. If the voxels are marked twice, the voxels $c_{ijk}(x_i, y_j, z_k)$ are included in the candidate list of occluded voxels.
Step 3: If the neighborhood voxels (top, bottom, left, and right) of candidates existed in the candidate list or the edge voxels of the tree, the candidates remain in the candidate list. Otherwise, the candidates are removed from the list.
Step 4: Step 3 is repeated until the number of candidates in the list remain unchanged. The candidates in the list represent the occluded voxels of the 3D voxel model, as indicated by the red grids in Fig. 4 (d).

Compared to traditional 3D mathematical morphology and interpolation methods, the proposed method was less affected by individual voxels or voxel groups, such as noise or branch points, that were close to the contour of trunks and large branches (Gorte and Pfeifer, 2004; Hosoi et al., 2013). The area of the total interior filling in each section of the tree (S_{IFk}, m^2) could be calculated by counting the number of occluded voxels using Eq. (1).

$$S_{IF_k} = N_k \bullet l_v^2 \tag{1}$$

where N_k represents the number of occluded voxels in the k-th layer, and l_v(m) is the voxel size.

2.3.3. Refinement of edge voxels

To allocate all 3D points of the tree to voxels with a specific size, voxelization is performed (Fig. 5). However, the number and distribution of points in each voxel are uncertain, resulting in certain voxels being partially filled with points, leading to volume overestimation, especially for small branches. While using a small voxel size reduces the empty area in edge voxels to some extent, it also leads to the identification of more occluded voxels, resulting in heavier computation. Furthermore, voxelization fails when the voxel size is smaller than the point interval in the 3D point cloud.

Therefore, the voxel size should be adapted to the actual point distribution of the tree, especially for voxels at the edge of the 3D voxel model (Fig. 5c). To achieve this, an axis-parallel voxel-refinement method is developed. The equal grid of each edge voxel $c_{ijk}(x_i, y_j, z_k)$ filled with points of the tree in the k-th layer is converted to an axially aligned bounding box (AABB). This rectangle bounding box is used to define the boundary. The sides of AABB are parallel to the axis of coordinate system. The vertices $\{\min(c_{ijk}[x]), \max(c_{ijk}[x]), \min(c_{ijk}[y]),$

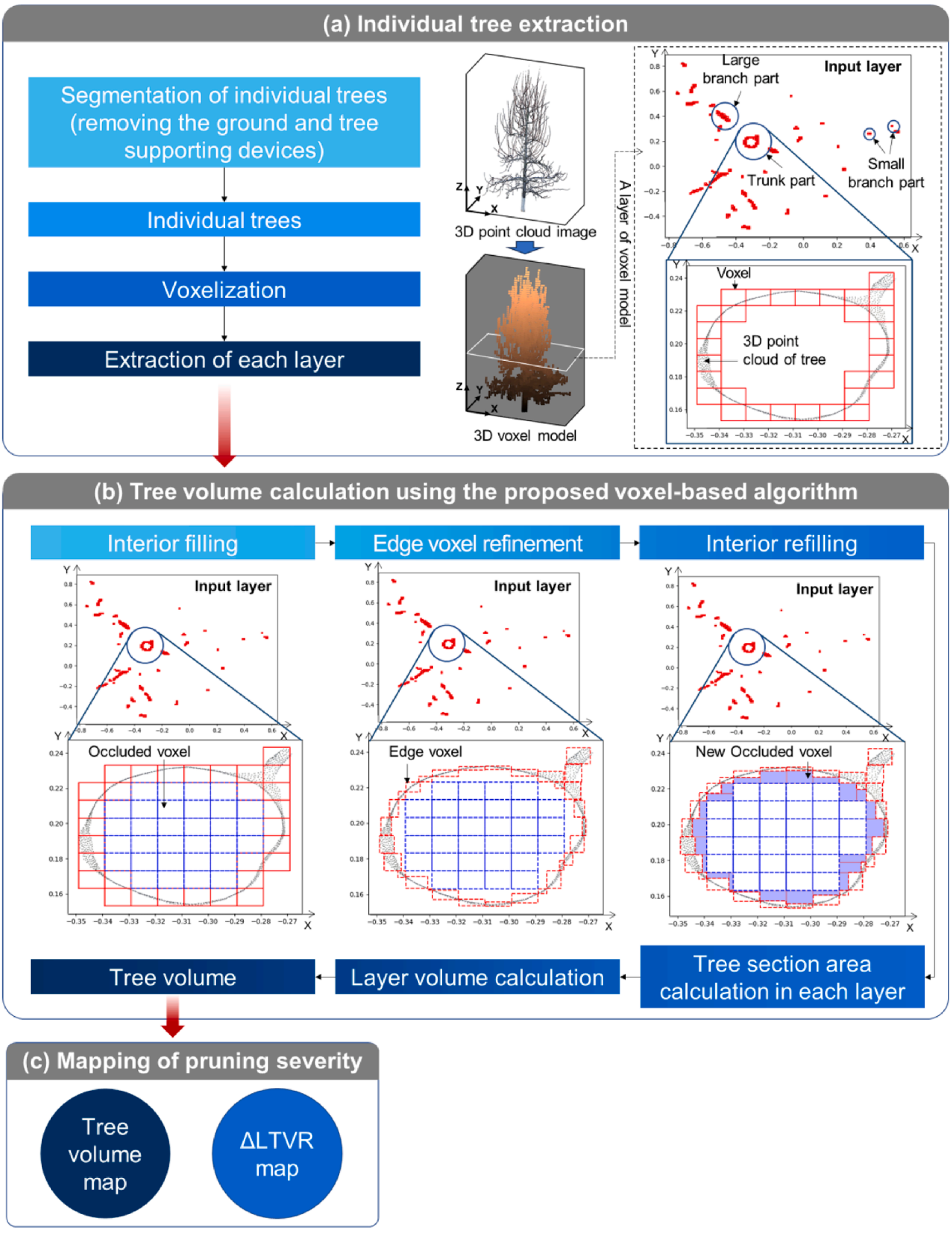

Fig. 3. Process of tree volume calculation and pruning severity mapping.

$\max(c_{ijk}[y])\}$ of AABB are based on the minimum and maximum projections of points in the voxels $c_{ijk}(x_i, y_j, z_k)$ along the X- and Y-directions, respectively. AABB can shrink the boundary of the equal grid of the voxel based on the shape of inner points in the axis direction as shown in the transformation from Fig. 5(b) to Fig. 5(c). However, if the neighborhood voxels (top, bottom, left, and right) of an edge voxel are also edge voxels, then this edge voxel will not participate in the refinement processing. The area of the refinement bounding box in the

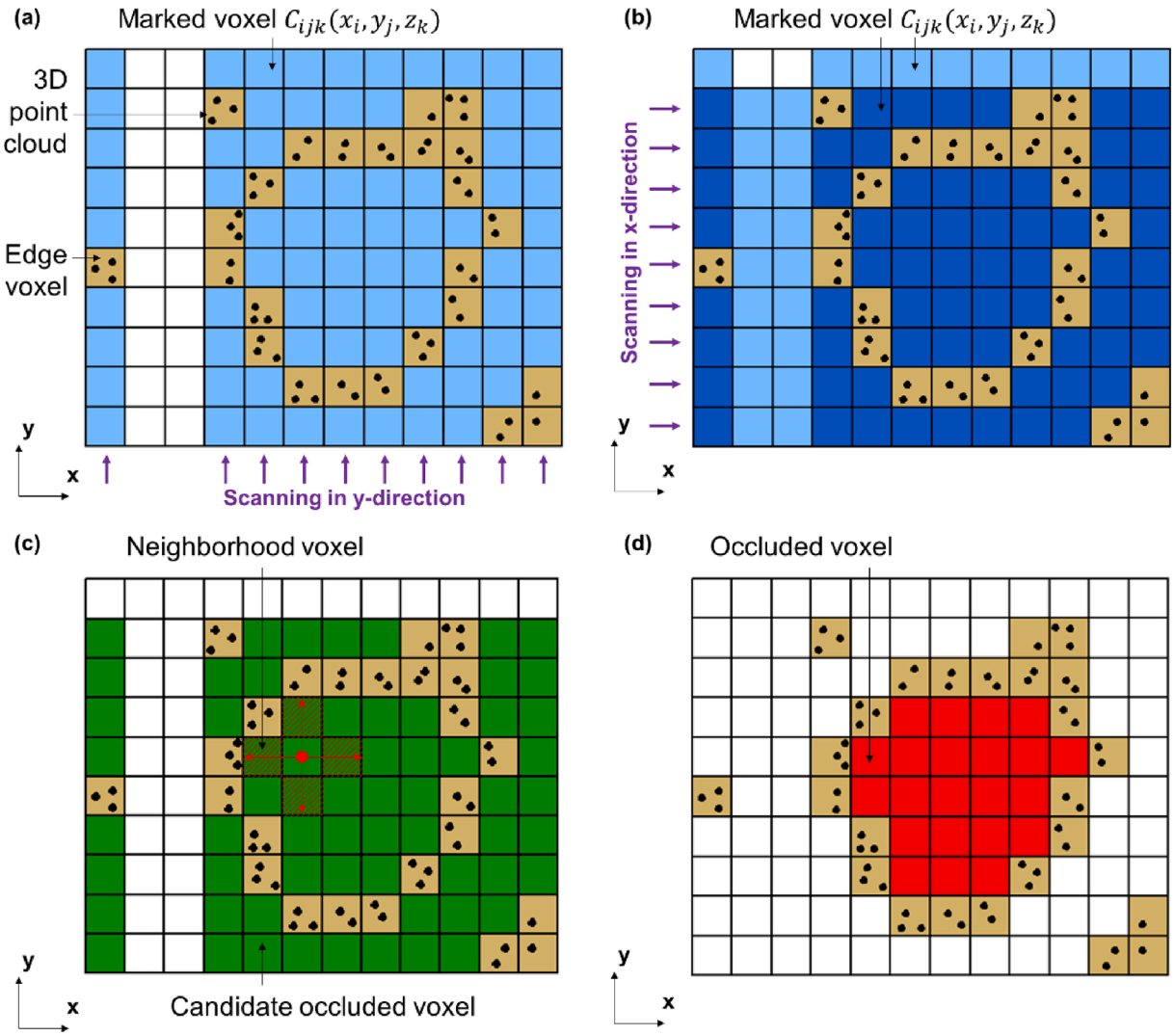

Fig. 4. Recognition of the occluded voxels in the voxel model: (a) scanning in y-direction, (b) scanning in x-direction, (c) candidates of the occluded voxels that are scanned in both y and x directions, and (d) identification of the occluded voxels.

k-th layer (S_{ET_k}, m^2) can be calculated as follows:

$$S_{ET_k} = \sum_{i,j} \left[\left| \max\left(c_{ijk}[x]\right) - \min\left(c_{ijk}[x]\right) \right| \bullet \left| \max\left(c_{ijk}[y]\right) - \min\left(c_{ijk}[y]\right) \right| \right] \quad (2)$$

where $\max(c_{ijk}[x])$ and $\min(c_{ijk}[x])$, and $\max(c_{ijk}[y])$ and $\min(c_{ijk}[y])$ denote the maximum and minimum values of the point set of the voxel $c_{ijk}(x_i, y_j, z_k)$ in the X- and Y-directions, respectively.

2.3.4. Interior refilling of the 3D voxel model

Refinement of the original voxels generates gaps between the thinned bounding boxes (red dashed box) and neighboring occluded (inner) voxels (blue box) (Fig. 6a). Interior refilling is performed to obtain a high-precision section area of the tree. For each refined voxel, the neighboring voxels are checked. If a side of the refined voxel is adjacent to an occluded voxel, it is marked with deep green lines, as shown in Fig. 6(a). The side of the refined bounding box is extended to the side face of the corresponding neighboring occluded voxel, as indicated by the arrows in Fig. 6(a). If the sides of the refined bounding box have more than one neighboring occluded voxel, the number of extending operations is based on the number of neighboring occluded voxels, and the extending order follows the clockwise direction (first extending by step ① and then step ② in Fig. 6a). The blue-filled rectangles in Fig. 6(b) indicate the areas of interior refilling, and no empty space exists between the refined bounding box and occluded voxels.

The vertex coordinates of the interior refilling rectangle can be defined in four different cases based on the position relation between the refined bounding box and neighboring occluded voxels.

Case 1: When the adjacent occluded voxel is located above the refined bounding box, the interior refilling rectangle can be determined using the upper-left (vertex 1) and lower-right (vertex 2) vertices, as shown in Fig. 7(a).

$$S_{RF\_up_k} = \sum_{i,j} \left[\left| \max\left(c_{ijk}[x]\right) - x_i \right| \bullet \left| \max\left(c_{ijk}[y]\right) - y_{j+1} \right| \right] \quad (3)$$

where $S_{RF\_up_k}$ (m^2) denotes the area of interior refilling in the k-th layer for case 1, and x_i and y_{j+1} represent the x and y coordinate values, respectively, of the voxel $c_{i(j+1)k}(x_i, y_{j+1}, z_k)$.

Case 2: When the adjacent occluded voxel is located at the right of the refined bounding box, the interior refilling rectangle can be determined using the upper-right (vertex 1) and lower-left (vertex 2) vertices, as shown in Fig. 7(b).

$$S_{RF\_r_k} = \sum_{i,j} \left[\left| \max\left(c_{ijk}[x]\right) - x_{i+1} \right| \bullet \left| \min\left(c_{ijk}[y]\right) - y_{j+1} \right| \right] \quad (4)$$

Where $S_{RF\_r_k}$ (m^2) indicates the area of interior refilling in the k-th layer for case 2, and x_{i+1} and y_{j+1} represent the x and y coordinate values,

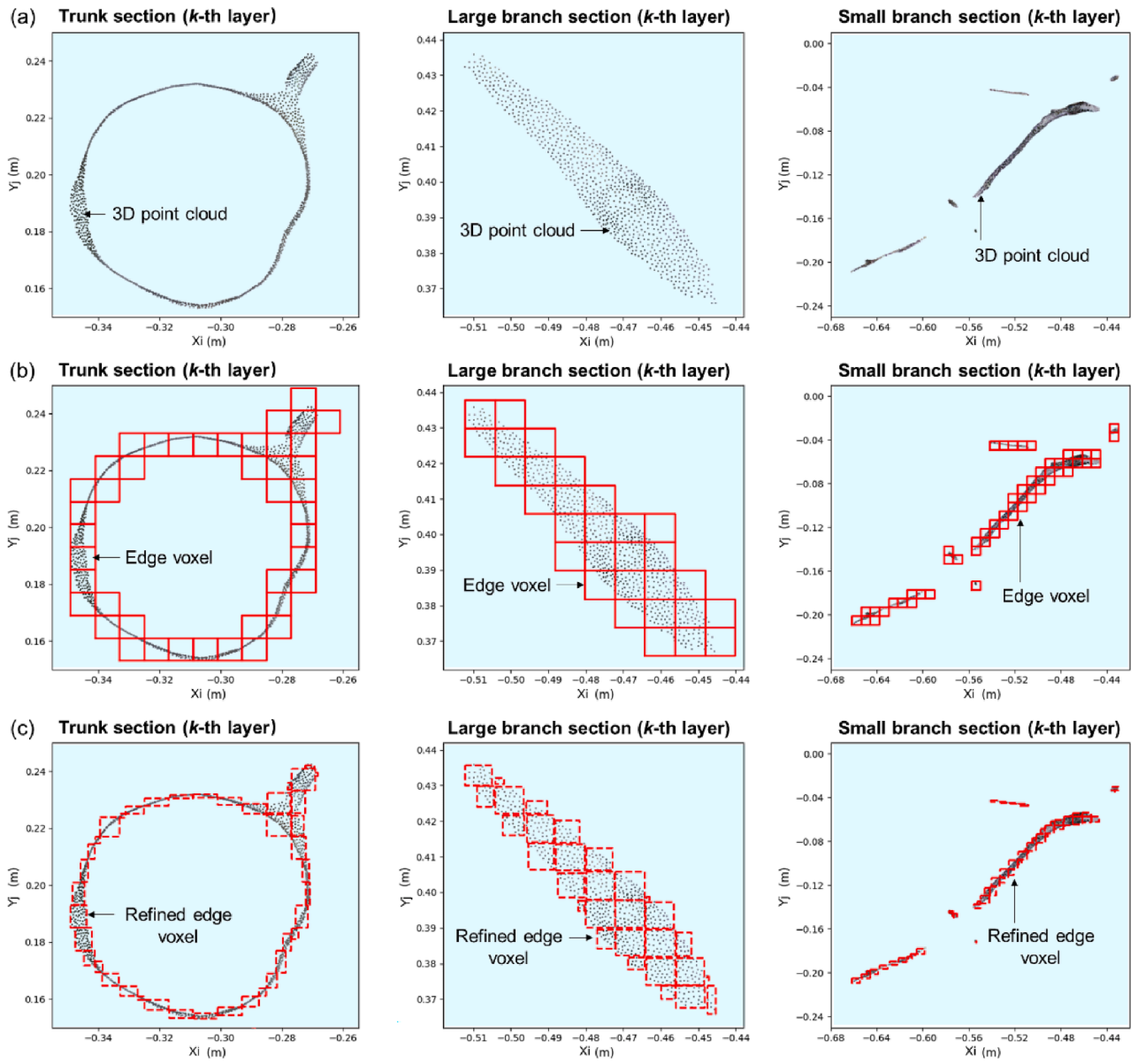

Fig. 5. Edge voxel refinement: (a) 3D point cloud of trunk, large branch, and small branch section, (b) voxelization of the 3D point cloud, and (c) refinement of the original voxels.

respectively, of the voxel $c_{(i+1)(j+1)k}(x_{i+1}, y_{j+1}, z_k)$.

Case 3: When the adjacent occluded voxel is located at the bottom of the refined bounding box, the interior refilling rectangle can be determined using the lower-right (vertex 1) and upper-left (vertex 2) vertices, as shown in Fig. 7(c).

$$S_{RF\_d_k} = \sum_{i,j} \left[\left| \min\left(c_{ijk}[x]\right) - x_{i+1} \right| \bullet \left| \min\left(c_{ijk}[y]\right) - y_j \right| \right] \quad (5)$$

where $S_{RF\_d_k}$ (m^2) denotes the area of interior refilling in the k-th layer for case 3, and x_{i+1} and y_j represent the x and y coordinate values, respectively, of the voxel $c_{(i+1)jk}(x_{i+1}, y_j, z_k)$.

Case 4: When the adjacent occluded voxel is located at the left of the refined bounding box, the interior refilling rectangle can be determined using the lower-left (vertex 1) and upper-right (vertex 2) vertices, as shown in Fig. 7(d).

$$S_{RF\_l_k} = \sum_{i,j} \left[\left| \min\left(c_{ijk}[x]\right) - x_i \right| \bullet \left| \max\left(c_{ijk}[y]\right) - y_j \right| \right] \quad (6)$$

where $S_{RF\_l_k}$ (m^2) indicates the area of interior refilling in the k-th layer for case 4, and x_i and y_j represent the x and y coordinate values, respectively, of the original voxel $c_{ijk}(x_i, y_j, z_k)$ of the thinned bounding box.

Therefore, the total interior refilling area (S_{RF_k}, m^2) in the k-th layer is obtained by adding the individual refilling areas in the four cases.

$$S_{RF_k} = S_{RF\_up_k} + S_{RF\_r_k} + S_{RF\_d_k} + S_{RF\_l_k} \quad (7)$$

2.3.5. Volume calculation using the proposed method

As discussed in the previous sections, the section area in each layer was corrected by applying interior filling of the 3D voxel model, thinning of edge voxels, and interior refilling of the 3D voxel model. The volume in the k-th layer (V_k, m^3) can be calculated based on the voxel size l_v (m) and the section area of interior filling, thinned edge voxels, and interior refilling using Eq. (8).

$$V_k = \left(S_{IF_k} + S_{ET_k} + S_{RF_k}\right) \bullet l_v \quad (8)$$

The total volume V (m^3) of the tree can be calculated by summing the volume of each layer.

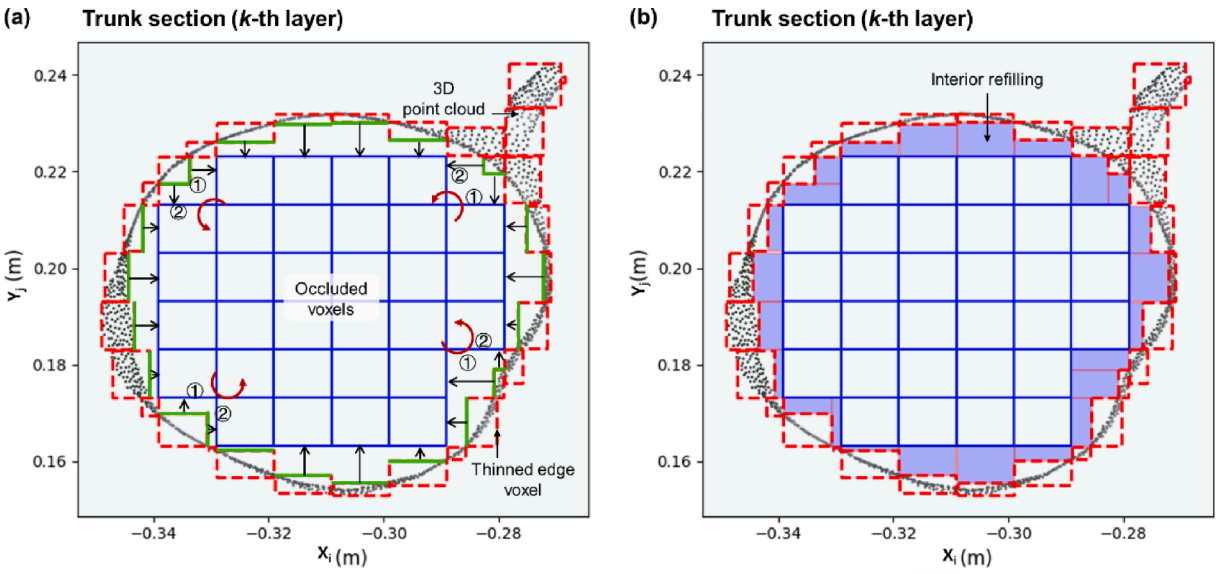

Fig. 6. Interior refilling of 3D voxel model: (a) extension of the sides of refined bounding boxes to the neighboring inner voxels, and (b) interior refilling section area of the truck section.

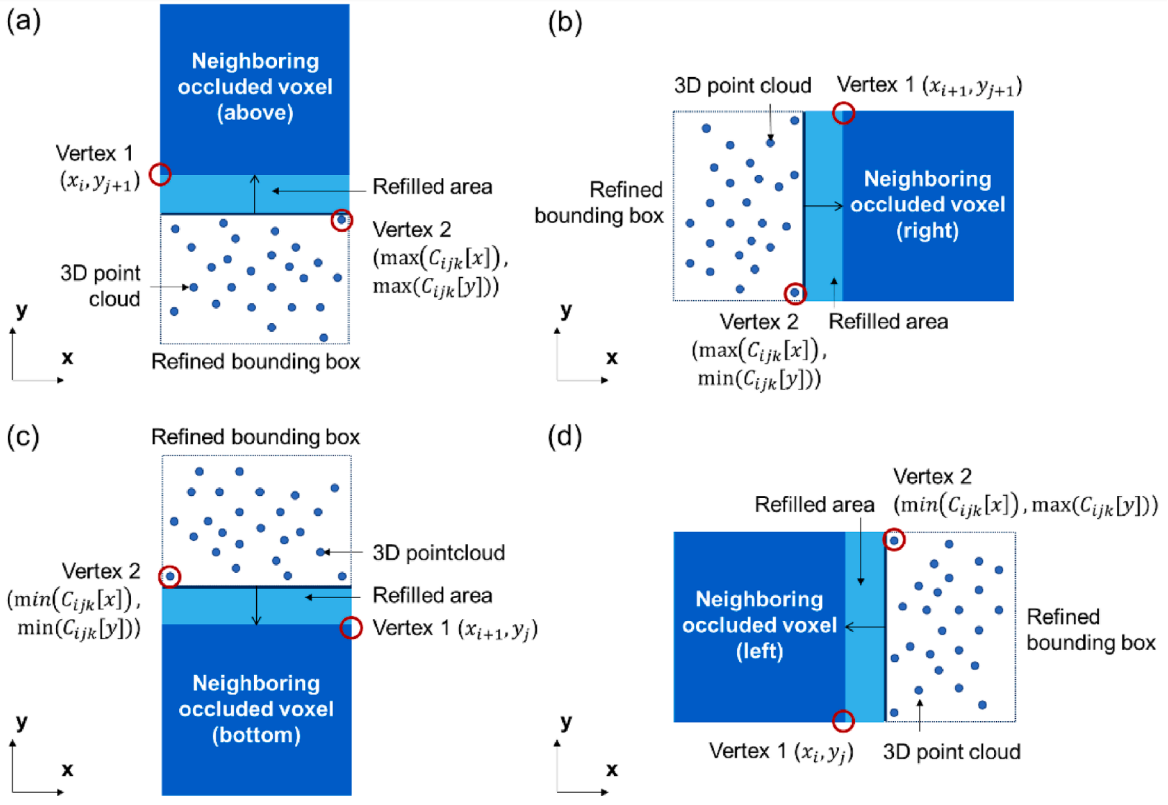

Fig. 7. Different conditions for calculation of the interior refilling area: (a) adjacent occluded voxel located above the refined bounding box (case 1), (b) adjacent occluded voxel located at the right of the refined bounding box (case 2), (c) adjacent occluded voxel located at the bottom of the refined bounding box (case 3), and (d) adjacent occluded voxel located at the left of the refined bounding box (case 4).

$$V = \sum_{k}^{N} V_k \tag{9}$$

where N denotes the number of layers depending on the voxel size l_v. The small voxel size results in a precise voxelization model with more layers.

The trunk, which is the central wooden axis of the tree from bottom to top, was distinguished from the rest of the tree, which is considered to be the branches. To calculate the LTVR, the 3D point cloud of the tree was separated into the trunk and branch parts. The LTVR of each tree can be obtained using Eq. (10).

$$LTVR = \frac{V_B}{V_T} \tag{10}$$

where V_B (m^3) and V_T (m^3) denote the volume of branch and trunk in each tree, respectively.

2.4. Evaluation and statistical analysis

2.4.1. Evaluation of tree volume measurement

To validate the performance of the proposed tree volume calculation algorithm, seven trees of different sizes were selected, and the mean absolute percentage error (MAPE) was computed using Eq. (11).

$$MAPE = \frac{\sum_n^N \frac{|V_n - \overline{V}_n|}{\overline{V}_n}}{N} \times 100\% \quad (11)$$

where V_n (m^3) denotes the calculated volume using the proposed algorithm, $\overline{V_n}$ (m^3) represents the ground truth of the tree volume measured by the water displacement method, and N represents the number of trees used for testing. The water displacement method calculates the tree volume by manually measuring the change in water level in a water-filled gauged cylinder after completely submerging the chopped tree in the cylinder. Before manual measurement, the selected trees were divided into trunk and branch parts, and the volume of each part was measured. The volume of the whole tree was obtained by summing up the volumes of the trunk and branch parts. The MAPE for the volume estimation of the trunk and branch parts was also calculated using Eq. (11). Additionally, to validate the correlation between the estimated volume and the ground truth, the coefficient of determination (R^2), the root mean squared error (RMSE), and the relative root mean squared error (rRMSE), presented in Eq. (12), of the linear regression were calculated. The rRMSE, which represents the normalization of the RMSE, allows for the comparison of errors across different methods while minimizing the impact of the object scale problem.

$$rRMSE = \frac{RMSE}{\frac{1}{N}\sum_n^N \overline{V_n}} \times 100\% \quad (12)$$

As the proposed algorithm was voxel-based, the voxel size was an influencing parameter for the accuracy and efficiency of volume calculation. Therefore, we optimized the voxel size by minimizing the RMSE.

2.4.2. Statistical analysis of ΔLTVR

The pruning severity of different pruning methods commonly used in orchards was evaluated by analyzing the variation in LTVR. The change in the volume of individual trunk and branch parts of trees in the experimental field was calculated using the proposed algorithm based on the pre- and post-pruning 3D data. The difference in LTVR (ΔLTVR) before and after tree pruning was examined using two-way analysis of variance (ANOVA) with two parameters, the tree pruning method and planting interval. The ΔLTVR values were then mapped onto the orchard image and visualized as pruning severity.

3. Results and discussion

3.1. Voxel size optimization

The voxel size used in the voxel-based volume calculation method is a crucial input parameter. When the voxel size is reduced, the 3D point cloud is converted into a highly refined 3D voxelization model with numerous voxels, as seen in the voxelization models with different voxel sizes in Fig. 8(a). However, this also increases the number of occluded

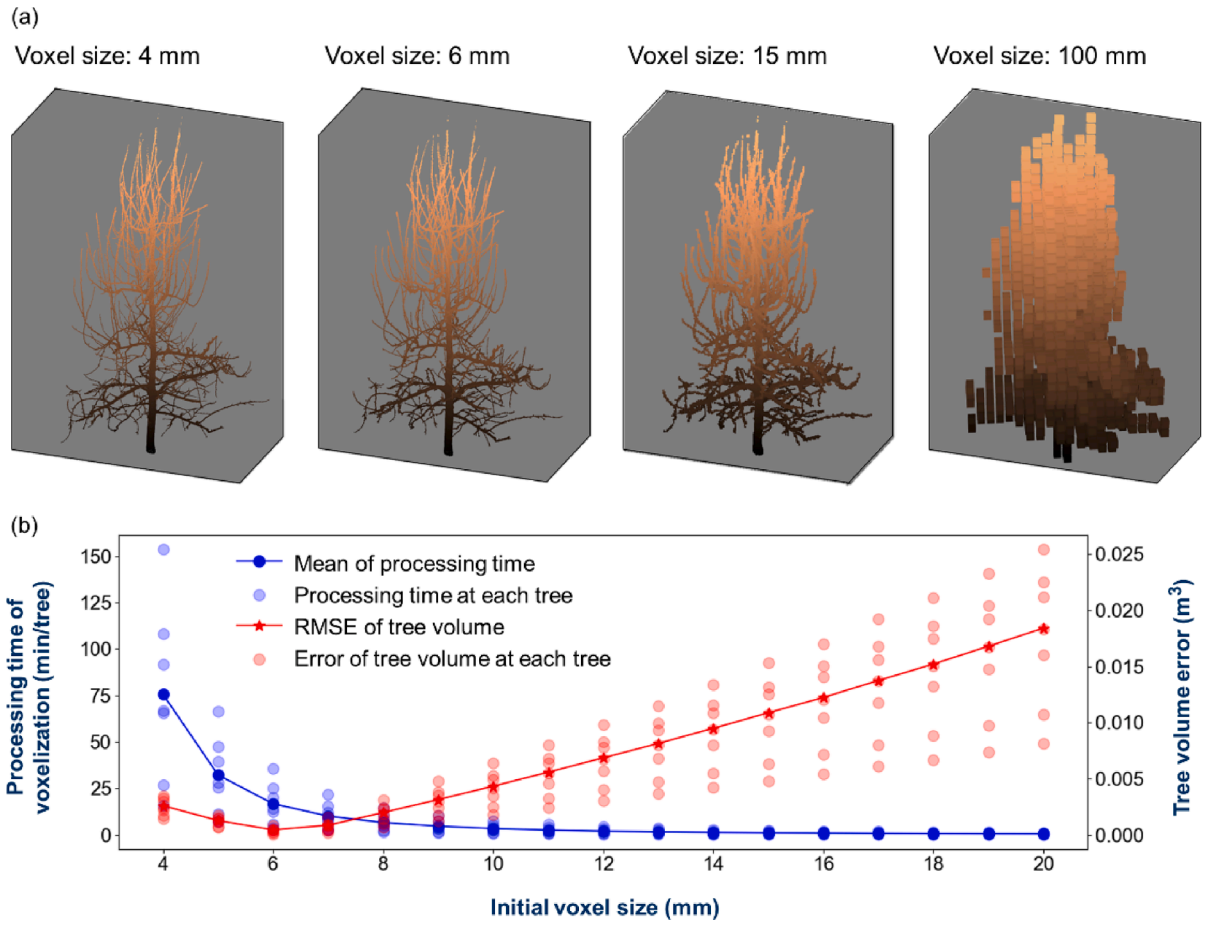

Fig. 8. Characteristics of voxelization with different voxel sizes: (a) 3D voxelization model with various voxel sizes, and (b) processing time of voxelization and error of tree volume estimation at different initial voxel sizes across seven trees.

voxels in the trunk and large branches that do not contain any tree points, which are missed in the volume calculation. Conversely, edge voxels are directly dependent on voxel size and become more accurate for volume calculation as the voxel size decreases. The conventional voxelization method does not account for voxel size, resulting in a hollow voxelization model with small voxel sizes and a redundant voxelization model with large voxel sizes, as shown in Fig. 8(a).

With a variation in the initial voxel size, the error in volume estimation differs as empty areas still exist in the refined edge voxels. Fig. 8 (b) shows the RMSE values of tree volume estimation with different initial voxel sizes ranging from 4 mm to 20 mm represented by a red line. The RMSE of volume estimation is observed to decrease with a decrease in the initial voxel size to 6 mm, and then it increases with an increase in voxel size. However, it is noticed that when the voxel sizes are less than 6 mm, the tree volume is underestimated. This happens because the minimum space between adjacent 3D point clouds results in an empty space between adjacent refined bounding boxes that belong to the tree and are not considered in volume calculation. As the voxel size approaches or becomes less than the minimum space, more empty area is generated between the new adjacent refined edge voxels, leading to underestimation of the tree volume. Based on the RMSE analysis, the volume calculation with a voxel size of 6 mm achieves the highest accuracy. Furthermore, Fig. 8(b) shows that the processing time decreases with larger voxel sizes. The running time decreased more gradually for voxel sizes larger than 6 mm. Considering both the error in volume estimation and the processing time for voxelization, an initial voxel size of 6 mm is selected for estimating the volume of apple trees, maintaining a minimum space of 1 mm between 3D points.

3.2. Comparison of the proposed algorithm with established methods

Fig. 9 presents the linear regressions of the tree volume estimation: the ground truth comparison with the voxelization methods with different voxel sizes is depicted. These methods include conventional voxelization with voxel sizes of 20 mm and 6 mm, and the proposed method, which utilizes an initial voxel size of 6 mm. The volume estimation by the proposed method is close to the ground truth ($R^2 = 0.994$, MAPE = 2.919 %). The conventional voxelization method is influenced by the voxel size. In this study, the conventional voxelization method with a voxel size of 6 mm (RMSE = 0.0089 m^3) exhibits a lower error than that with a voxel size of 20 mm (RMSE = 0.1114 m^3). However, it is still difficult to determine the optimum voxel size due to different and uncertain object structures.

The proposed voxelization method for tree volume measurement shows superior performance compared to the conventional methods. The proposed algorithm involves interior filling, edge voxel refinement, and interior refilling, resulting in a complete 3D voxelization model. Unlike the conventional voxelization methods, the proposed method can decrease the error of volume calculation at each step, as shown in Fig. 10. The gray-colored bar represents the tree volume measurement

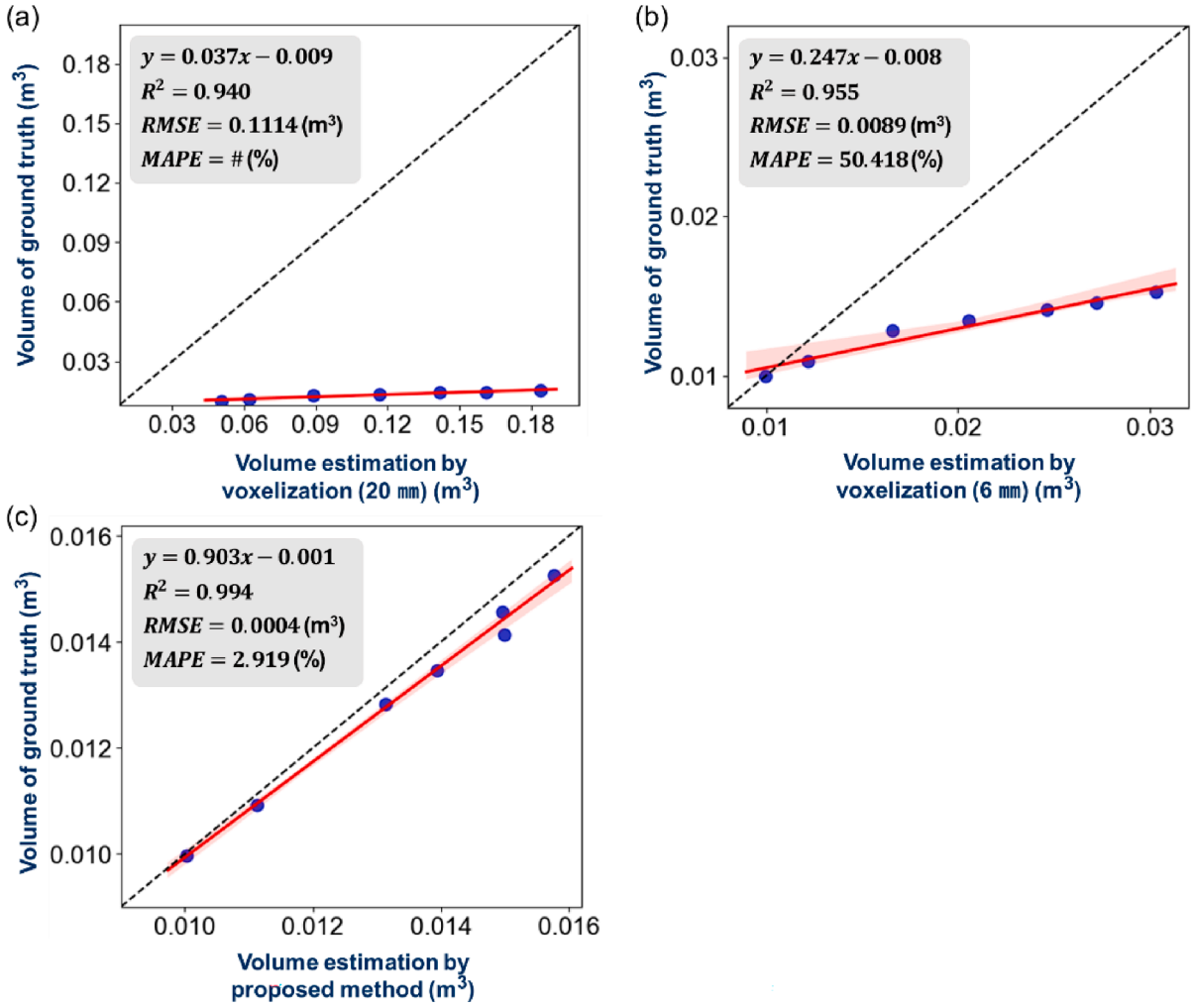

Fig. 9. Linear regression analysis of tree volume estimation: (a) and (b) conventional voxelization method with a voxel size of 20 and 6 mm, respectively, and (c) the proposed method with an initial voxel size of 6 mm. The symbol "#" indicates an extreme MAPE value that is greater than 100 %. The shaded area represents a 95 % confidence interval.

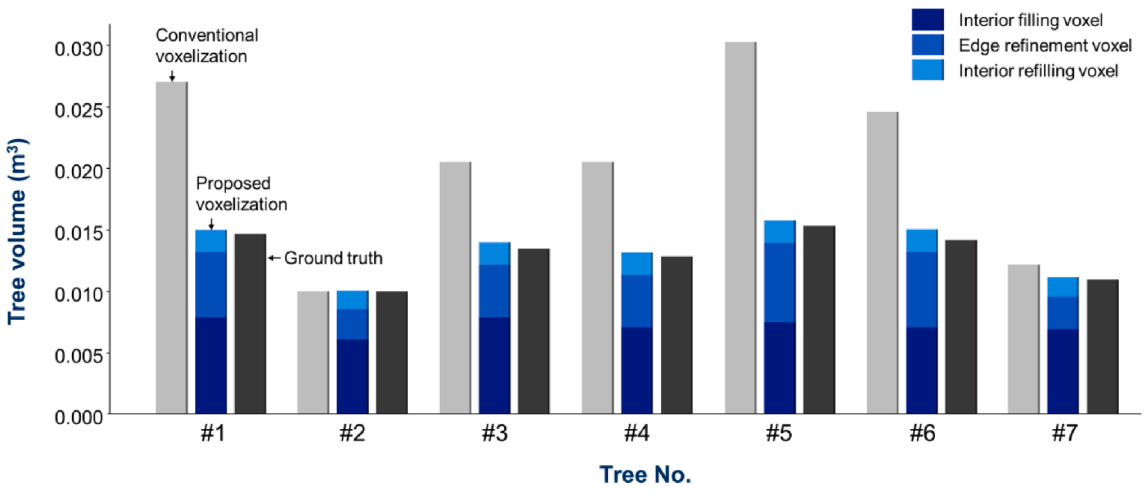

Fig. 10. Tree volume measurement by the conventional voxelization method with a voxel size of 6 mm, the proposed voxelization method at each step of interior filling, edge refinement, and interior refilling with an initial voxel size of 6 mm, and ground truth of tree volume.

using the conventional voxelization method with a voxel size of 6 mm. Since the cloud points of trees are not evenly distributed in the edge voxels, refining edge voxels in the proposed method can contribute to reducing the volume measurement. The dark blue and light blue bars represent the volumes obtained by interior filling and edge refinement in the proposed method, respectively. The dark blue bar reflects the volume of the tree trunk and large branches, which have similar volumes across the trees since they were trained using the same apple tree system. The light blue bar mainly reflects the volume of small branches, which shows some variation across trees.

In this study, the pruning severity index is defined as LTVR, which represents the volume ratio of the branch to the trunk. Therefore, accurate estimations of tree trunk and branch volume are necessary. The individual volumes of the trunk and branches were measured using the proposed algorithm with an initial voxel size of 6 mm. The linear regressions of the trunk and branch measurements with the ground truth are analyzed, as shown in Fig. 11. The accuracies of the trunk and branch volume estimations are approximately 97 % (MAPE = 2.94 %) with an RMSE of 0.0004 m^3 and approximately 94 % (MAPE = 5.57 %) with an RMSE of 0.0002 m^3, respectively. Compared to the results reported by Hosoi et al. (2013), the accuracy of branch volume estimation by the proposed method is much higher than that (approximately 64 %) of the Hosoi method, which only considered inner filling processing. In the proposed method, the inner empty area of the 3D voxelization model was fully filled, and thus the primary error of volume estimation was from the volume of edge voxels. If the surface of the 3D point cloud is more complex, a greater number of edge voxels will be generated during the initial voxelization step. Therefore, edge voxel refinement and interior refilling become crucial for accurately measuring the tree volume, particularly in trees with complex surface characteristics. Given that the trunk tends to have a thicker and simpler shape compared to the branches, the error in refining the edge voxels is lower for the trunk. Consequently, the overall error in the tree volume estimation is also lower for the trunk compared to the branches, as depicted in Fig. 11.

To assess the accuracy of the proposed method, we compared its performance with that of three established methods: AdQSM (Fan et al., 2020b), a skeleton-based method (Fan et al., 2023), and Allometric Scaling Models (ASM) (Bornand et al., 2023), as detailed in Table 1. These methods are utilized for reconstructing 3D point clouds of trees and calculating tree volume. Tree volume estimation is commonly conducted in the forestry domain, where the objects are larger than the fruit trees examined in our study. Consequently, the RMSE for these methods can be significantly higher than that for fruit trees. To mitigate this scale discrepancy, we employed the rRMSE.

Our evaluation showed that the proposed method surpassed the other three methods in terms of tree volume estimation accuracy. The

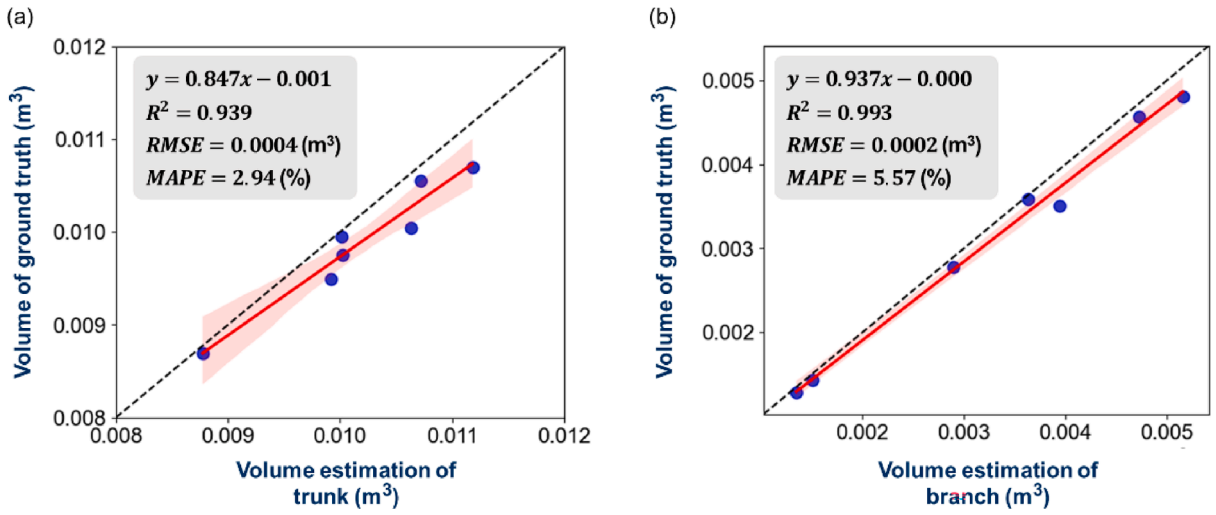

Fig. 11. Linear regression of the tree trunk and branch volume estimation between the proposed method and the ground truth: (a) volume estimation of trunk, and (b) volume estimation of branch. The shaded areas indicate a 95% confidence interval.

Table 1
Comparison of the proposed method and established methods for tree volume estimation.

Method	rRMSE (%)		
	Whole tree	Stem	Branch
AdQSM	22.62	–	36.86
Skeleton-based method	–	19.00	38.84
ASM	25.39	23.71	153.51
Proposed method	3.07	4.05	6.38

AdQSM, an advanced version of QSM, excels in reconstructing tree structures and, as a result, provides more accurate tree volume estimations than the other two methods. The effectiveness of the skeleton-based method heavily relies on the quality of input data and the skeletonization algorithm, which leads to moderate performance. Conversely, the ASM, a mathematical model designed for estimating the volume or biomass of a plant or animal based on size or specific measurements, demonstrated robustness in estimating the volume of convex-shaped objects like stems and canopies. However, its accuracy in predicting the volume of branches, typically concave-shaped and complex, was less reliable.

In summary, the proposed method, by focusing on the distribution of the point cloud rather than the tree's structure, enables precise volume estimation. By fine-tuning the voxel size to better match the point cloud distribution, the proposed method can accurately estimate the volume of not only large objects like the whole tree but also smaller components such as branches.

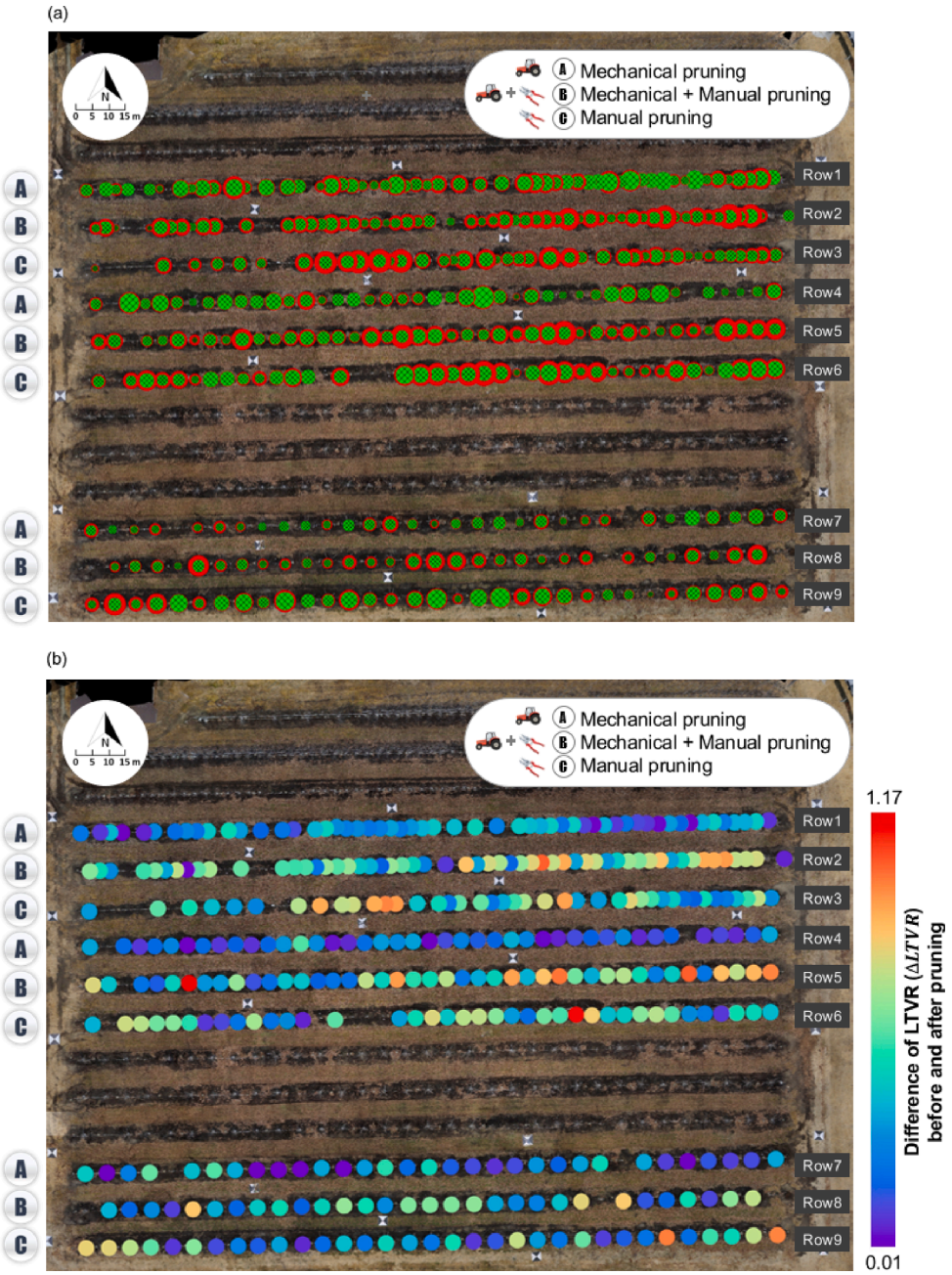

Fig. 12. Tree pruning severity map: (a) the tree volume removed by different pruning methods, where the green solid circles with mesh patterns represent the tree volume retained after pruning, and the red annulus represents the volume removed by pruning, and (b) ΔLTVR of trees before and after pruning using different methods. (For interpretation of the references to colour in this figure legend, the reader is referred to the web version of this article.)

3.3. Pruning severity mapping

In this study, a method was proposed to estimate the volumes of apple trees removed by pruning. The resulting volumes were projected onto an orchard map, as shown in Fig. 12(a). The green solid circles with mesh patterns represent the tree volume retained after pruning, while the red annulus regions indicate the volume removed by pruning. The total volume of each tree is the sum of the green solid circle and red annulus areas, which can directly reflect the growth status of the tree. The mechanical method shows less severity in pruning compared to the combination of mechanical and manual methods, and the manual method alone. This is indicated by the smaller red circular area in the mechanical method compared to the other two methods. The combination of mechanical and manual methods prunes individual trees more precisely, resulting in a more uniform distribution of the red annulus on most of each tree. The tree interval is different, with 1 m (rows 1–3), 1.5 m (rows 4–6), and 2 m (rows 7–9), which can be clearly recognized in the tree volume map (Fig. 12a). The pruning severity at the tree interval of 2 m is found to be less severe than that at 1 m and 1.5 m. Fig. 12(b) illustrates the difference in pruning index LTVR (ΔLTVR) before and after pruning at each tree. In general, the ΔLTVR value in the mechanical method is smaller than that in the combination of mechanical and manual pruning methods and the manual method alone, indicating less pruning severity in the mechanical method compared to the other two methods. The pruning severity at the tree interval of 2 m (rows 7–9) is found to be less severe than that at 1 m (rows 1–3) and 1.5 m (rows 4–6), which agrees with the results found in the tree volume map (Fig. 12a). Quantitative analysis of the pruning severity map enables the design of pruning strategies that optimize sunlight irradiation and enhance tree vigor based on the specific conditions of the orchard.

3.4. Statistical analysis of pruning methods and tree intervals

Based on the 3D reconstruction technology and the proposed volume calculation method, it was possible to calculate the pruning index LTVR of trees in the orchard. The ΔLTVR before and after pruning was obtained and used to quantitatively describe the pruning severity of each pruning method on trees. Additionally, the trees were planted at three different intervals (1, 1.5, and 2 m). The significance difference of the pruning methods and the tree intervals were analyzed using two-way ANOVA, as shown in Fig. 13.

The mean ΔLTVR value of the combination of mechanical and manual pruning methods is the highest at all tree intervals, indicating that this method removes the most branches. In contrast, the mechanical pruning method shows the lowest ΔLTVR value, indicating that the volume of branches removed by this method is the least. This is because the mechanical method removes only the branches that can be reached by the cutting machine in a fixed position, and the volume of the removed branches depends on the selected cutting system area. On the other hand, the manual method is performed by growers based on their experience in pruning apple trees to achieve illumination and vigor balance. The combination of mechanical and manual methods involves first removing branches on the surface of the tree using the machine and then manually removing branches inside the tree.

In the ANOVA analysis, there is a significant difference between the combination of mechanical and manual pruning methods and the mechanical method alone at all tree intervals. The manual method shows a significant difference with the mechanical method at the tree interval of 1 m and 1.5 m, while there is no significant difference at 2 m. There is no significant difference between the combination of mechanical and manual pruning methods and the manual method alone at all tree intervals. In the statistical analysis of tree intervals, there is a significant difference between 1 m and 2 m, while there is no significant difference between the closest tree intervals. Regarding the manual pruning method, the mean ΔLTVR value is the lowest at the tree interval of 2 m compared to the other two intervals. The space of 2 m between adjacent

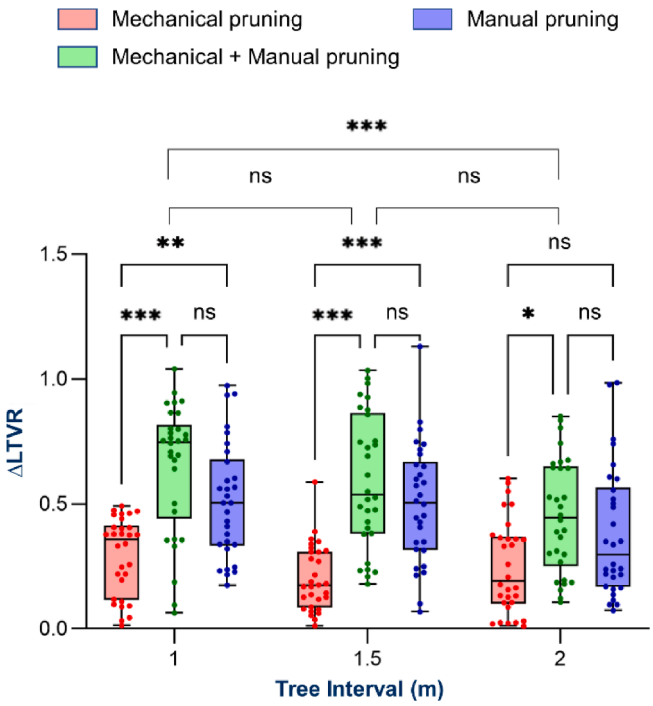

Fig. 13. Two-way ANOVA of the Δ*LTVR* with the three pruning methods and the three tree intervals. "*," "**," and "***" represent P value < 0.05, P value < 0.01, and P value < 0.001, respectively.

apple trees might be sufficient for illumination and tree vigor; thus, during manual pruning the grower might reduce the volume of the branches to be removed. The results of the statistical analysis shown in Fig. 13 agree well with those analyzed in the tree pruning severity map shown in Fig. 12.

4. Limitations and future work

The novel voxel-based algorithm developed in this study for measuring tree volume, which includes interior filling, edge voxel refinement, and interior refilling processes, has demonstrated superior performance compared to established methods. However, there are certain limitations and areas for future improvement that should be addressed.

One limitation of the voxel-based algorithm is the need to predetermine the initial voxel size, which was manually optimized in this study by comparing measurement errors and processing speed for different voxel sizes on a single tree. However, since the optimal initial voxel size can vary depending on the geometric characteristics of individual trees, it is necessary to develop an automatic optimization method that considers the unique geometric features of each tree. Integration of artificial intelligence technology can be explored to automate the optimization process for determining the initial voxel size.

In this study, several preprocessing steps for voxelizing the 3D point cloud, such as background removal, individual tree extraction, downsampling, and noise elimination, were performed manually using commercial software in separate steps. To expedite the commercialization of the voxel-based method, it is essential to integrate these preprocessing steps and the developed algorithm into a single software package for streamlined and efficient tree volume measurement.

The experiments conducted in this study focused on a single type of apple tree. To generalize the algorithm and ensure its applicability to a broader range of scenarios, further experiments should be conducted on different types of apple trees with varying geometric characteristics, as well as on various other fruit trees like pear, peach, and orange.

Another limitation is that tree volume measurements were

performed only during the leafless period to estimate pruning severity using different pruning methods. However, extending the application of the voxel-based algorithm to measure tree biomass during the leafy growth period would enable monitoring of tree vitality at each stage of growth. By incorporating tree vitality measurements, optimized treatments on individual trees can be applied at different growth stages, leading to improvements in fruit yield and quality.

Addressing these limitations and pursuing future work in these areas will enhance the practicality, versatility, and effectiveness of the voxel-based algorithm for tree volume measurement, benefiting orchard management practices and fruit production outcomes.

5. Conclusions

In this study, a high-quality 3D model of an apple orchard was reconstructed using a lightweight multi-camera platform and 3D photogrammetry technology. The resulting 3D point cloud data were utilized to calculate tree volume and determine pruning severity based on the LTVR index. This was accomplished using a novel voxel-based volume calculation algorithm that involved interior filling, edge voxel refinement, and interior refilling. To validate the algorithm, the volumes of seven apple trees were calculated using the proposed algorithm, and the obtained results were compared with those of three established methods. The results demonstrated that the proposed voxel-based algorithm was the most suitable for accurately calculating individual tree volumes using 3D point clouds. Additionally, the estimation of trunk and branch volumes using the proposed method yielded highly accurate results. Furthermore, tree volume and LTVR mapping using the obtained volume data for each tree were performed to visualize pruning severity. The analysis of the pruning severity map can facilitate the development of customized pruning strategies that account for the unique characteristics of the orchard, aiming to optimize sunlight exposure and enhance tree vitality. In the future, the extension of the voxel-based algorithm to measure tree biomass during the leafy growth period would facilitate the monitoring of tree vitality at each stage of growth, thereby enhancing orchard management practices and improving fruit production outcomes.

CRediT authorship contribution statement

Xuhua Dong: Data curation, Formal analysis, Visualization, Writing – original draft. **Woo-Young Kim:** Data curation, Investigation, Methodology. **Zheng Yu:** Data curation, Formal analysis, Investigation. **Ju-Youl Oh:** Investigation, Methodology, Supervision. **Reza Ehsani:** Supervision, Validation, Writing – review & editing. **Kyeong-Hwan Lee:** Conceptualization, Data curation, Formal analysis, Funding acquisition, Methodology, Supervision, Writing – review & editing.

Declaration of competing interest

The authors declare that they have no known competing financial interests or personal relationships that could have appeared to influence the work reported in this paper.

Data availability

Data will be made available on request.

Acknowledgments

This work was supported by Korea Institute of Planning and Evaluation for Technology in Food, Agriculture and Forestry (IPET) through the Advanced Agricultural Machinery Industrialization Technology Development Program (32003003) and the Open Field Smart Agriculture Technology Short-term Advancement Program, funded by Ministry of Agriculture, Food and Rural Affairs (MAFRA) (32204003).

References

Bienert, A., Hess, C., Maas, H.G., Von Oheimb, G., 2014. A voxel-based technique to estimate the volume of trees from terrestrial laser scanner data. Int. Arch. Photogrammetry, Remote Sensing Spatial Information Sciences 40 (5), 101. https://doi.org/10.5194/isprsarchives-XL-5-101-2014.

Bornand, A., Rehush, N., Morsdorf, F., Thürig, E., Abegg, M., 2023. Individual tree volume estimation with terrestrial laser scanning: Evaluating reconstructive and allometric approaches. Agric. For. Meteorol. 341, 109654 https://doi.org/10.1016/j.agrformet.2023.109654.

Bucksch, A., Lindenbergh, R., Menenti, M., 2010. SkelTre: Robust skeleton extraction from imperfect point clouds. Vis. Comput. 26, 1283–1300. https://doi.org/10.1007/s00371-010-0520-4.

Burt, A., Boni Vicari, M., Da Costa, A.C., Coughlin, I., Meir, P., Rowland, L., Disney, M., 2021. New insights into large tropical tree mass and structure from direct harvest and terrestrial lidar. R. Soc. Open Sci. 8 (2) https://doi.org/10.1098/rsos, 201458.

Chen, Z., Tagliasacchi, A., Funkhouser, T., Zhang, H., 2022. Neural Dual Contouring. ACM Trans. Graph. 41, 1–13. https://doi.org/10.1145/3528223.3530108.

Demol, M., Calders, K., Krishna Moorthy, S.M., Van den Bulcke, J., Verbeeck, H., Gielen, B., 2021. Consequences of vertical basic wood density variation on the estimation of aboveground biomass with terrestrial laser scanning. Trees - Struct. Funct. 35 (2), 671–684. https://doi.org/10.1007/s00468-020-02067-7.

Demol, M., Calders, K., Verbeeck, H., Gielen, B., 2021b. Forest above-ground volume assessments with terrestrial laser scanning: a ground-truth validation experiment in temperate, managed forests. Ann. Botany 128 (6), 805–819. https://doi.org/10.1093/aob/mcab110.

Fan, G., Nan, L., Chen, F., Dong, Y., Wang, Z., Li, H., Chen, D., 2020a. A New Quantitative Approach to Tree Attributes Estimation Based on LiDAR Point Clouds. Remote Sens. 12, 1779. https://doi.org/10.3390/rs12111779.

Fan, G., Nan, L., Dong, Y., Su, X., Chen, F., 2020b. AdQSM: A New Method for Estimating Above-Ground Biomass from TLS Point Clouds. Remote Sens. 12, 3089. https://doi.org/10.3390/rs12183089.

Fan, G., Lu, F., Cai, H., Xu, Z., Wang, R., Zeng, X., Xu, F., Chen, F., 2023. A New Method for Reconstructing Tree-Level Aboveground Carbon Stocks of Eucalyptus Based on TLS Point Clouds. Remote Sens. 15, 4782. https://doi.org/10.3390/rs15194782.

Girardeau-Montaut, D., 2016. CloudCompare. EDF R&D Telecom ParisTech, France.

Gorte, B., Pfeifer, N., 2004. Structuring laser-scanned trees using 3D mathematical morphology. International Archives of Photogrammetry and Remote Sensing 35 (B5), 929–933.

Han, X.F., Jin, J.S., Wang, M.J., Jiang, W., Gao, L., Xiao, L., 2017. A review of algorithms for filtering the 3D point cloud. Signal Process. Image Commun. 57, 103–112. https://doi.org/10.1016/j.image.2017.05.009.

He, L., Schupp, J., 2018. Sensing and automation in pruning of apple trees: A review. Agronomy 8 (10), 211. https://doi.org/10.3390/agronomy8100211.

Hosoi, F., Nakai, Y., Omasa, K., 2013. 3-D voxel-based solid modeling of a broad-leaved tree for accurate volume estimation using portable scanning lidar. ISPRS J. Photogramm. Remote Sens. 82, 41–48. https://doi.org/10.1016/j.isprsjprs.2013.04.011.

Hutchison, D., Kanade, T., Kittler, J., Kleinberg, J.M., Mattern, F., Mitchell, J.C., Naor, M., Nierstrasz, O., Pandu Rangan, C., Steffen, B., Sudan, M., Terzopoulos, D., Tygar, D., Vardi, M.Y., Weikum, G., Zhou, Q.-Y., Neumann, U., 2010. 2.5D Dual Contouring: A Robust Approach to Creating Building Models from Aerial LiDAR Point Clouds, in: Daniilidis, K., Maragos, P., Paragios, N. (Eds.), Computer Vision – ECCV 2010, Lecture Notes in Computer Science. Springer Berlin Heidelberg, Berlin, Heidelberg, pp. 115–128. Doi: 10.1007/978-3-642-15558-1_9.

Kankare, V., Holopainen, M., Vastaranta, M., Puttonen, E., Yu, X., Hyyppä, J., Alho, P., 2013. Individual tree biomass estimation using terrestrial laser scanning. ISPRS J. Photogramm Remote Sens. 75, 64–75. https://doi.org/10.1016/j.isprsjprs.2012.10.003.

Krishna Moorthy, S.M., Raumonen, P., Van Den Bulcke, J., Calders, K., Verbeeck, H., 2020. Terrestrial laser scanning for non-destructive estimates of liana stem biomass. For. Ecol. Manage. 456, 117751 https://doi.org/10.1016/j.foreco.2019.117751.

Liu, Q., Xiao, J., Liu, L., Wang, Y., Wang, Y., 2023. High-Resolution and Efficient Neural Dual Contouring for Surface Reconstruction from Point Clouds. Remote Sens. 15, 2267. https://doi.org/10.3390/rs15092267.

Lordan, J., Pascual, M., Fonseca, F., Montilla, V., Papió, J., Rufat, J., Villar, J.M., 2015. An Image-based Method to Study the Fruit Tree Canopy and the Pruning Biomass Production in a Peach Orchard. HortSci. 50 (12), 1809–1817. https://doi.org/10.21273/HORTSCI.50.12.1809.

Mahmud, M.S., Zahid, A., He, L., Martin, P., 2021. Opportunities and Possibilities of Developing an Advanced Precision Spraying System for Tree Fruits. Sensors 21, 3262. https://doi.org/10.3390/s21093262.

Morgan, K.T., Scholberg, J.M.S., Obreza, T.A., Wheaton, T.A., 2006. Size, Biomass, and Nitrogen Relationships with Sweet Orange Tree Growth. J. Am. Soc. Hortic. Sci. 131, 149–156. https://doi.org/10.21273/JASHS.131.1.149.

Qi, Y., Dong, X., Chen, P., Lee, K.-H., Lan, Y., Lu, X., Jia, R., Deng, J., Zhang, Y., 2021. Canopy Volume Extraction of Citrus reticulate Blanco cv. Shatangju Trees Using UAV Image-Based Point Cloud Deep Learning. Remote Sens. 13, 3437. https://doi.org/10.3390/rs13173437.

Robinson, T.L., Lakso, A.N., Ren, Z., 1991. Modifying apple tree canopies for improved production efficiency. HortSci. 26 (8), 1005–1012. https://doi.org/10.21273/HORTSCI.26.8.1005.

Schupp, J.R., Winzeler, H.E., Kon, T.M., Marini, R.P., Baugher, T.A., Kime, L.F., Schupp, M.A., 2017. A method for quantifying whole-tree pruning severity in mature tall spindle apple plantings. HortSci. 52 (9), 1233–1240. https://doi.org/10.21273/HORTSCI12158-17.

Sun, S., Li, C., Chee, P.W., Paterson, A.H., Jiang, Y., Xu, R., Shehzad, T., 2020. Three-dimensional photogrammetric mapping of cotton bolls in situ based on point cloud segmentation and clustering. ISPRS J. Photogramm Remote Sens. 160, 195–207. https://doi.org/10.1016/j.isprsjprs.2019.12.011.

Tinkham, W.T., Swayze, N.C., 2021. Influence of Agisoft Metashape parameters on UAS structure from motion individual tree detection from canopy height models. Forests 12 (2), 250. https://doi.org/10.3390/f12020250.

Wang, Z., Lan, P., Sun, F. 2021. Correlation Research on the Structure of the Apple Tree Vigor and Its Fruit Quality. In New Developments of IT, IoT and ICT Applied to Agriculture (pp. 55-63). Doi: 10.1007/978-981-15-5073-7_6.

Xu, Y., Tong, X., Stilla, U., 2021. Voxel-based representation of 3D point clouds: Methods, applications, and its potential use in the construction industry. Autom. Constr. 126, 103675 https://doi.org/10.1016/j.autcon.2021.103675.

Yang, J., Wen, X., Wang, Q., Ye, J.-S., Zhang, Y., Sun, Y., 2022. A Novel Algorithm Based on Geometric Characteristics for Tree Branch Skeleton Extraction from LiDAR Point Cloud. Forests 13, 1534. https://doi.org/10.3390/f13101534.

You, A., Grimm, C., Silwal, A., Davidson, J.R., 2022. Semantics-guided skeletonization of upright fruiting offshoot trees for robotic pruning. Comput. Electron. Agric. 192, 106622 https://doi.org/10.1016/j.compag.2021.106622.

Zai-long, L. 1983. Control of fruit tree vigor by pruning. In International Workshop on Controlling Vigor in Fruit Trees 146 (pp. 277-286).